# Digital Predistortion of Millimeter-Wave GaN Power Amplifiers for 6G Integrated Communication, Sensing, and Power Transfer Scenarios

Yucheng Yu, *Graduate Student Member, IEEE*, Luqi Yu, *Graduate Student Member, IEEE*, Ruijia Liu, *Member, IEEE*, Xiao-Wei Zhu, *Member, IEEE*, Peng Chen, *Member, IEEE*, and Chao Yu, *Senior Member, IEEE*

***Abstract*— Aiming at supporting diverse applications, integrated communication, sensing, and power transfer (ICSPT) is anticipated to be a key feature of 6G networks. In ICSPT scenarios, power amplifiers (PAs) suffer from dynamic effects due to rapid switching between different operating modes, posing new challenges for PA linearization. In this article, a novel digital predistortion (DPD) method is proposed to effectively compensate for PA distortion in such scenarios. To accurately characterize these dynamic effects with low complexity, we introduce a method for calculating dynamic state variables that represent the dynamic behavior of PAs. For communication mode, these variables are incorporated into a neural network (NN) model, leveraging NN's powerful fitting capability to track changes in PA's nonlinear characteristics due to mode switching. For sensing and power transfer modes, the variables are used to fine-tune the input signal, compensating for fluctuations in PA's gain. Experimental validations were conducted on a millimeter-wave (mmWave) gallium nitride (GaN) PA at a center frequency of 27 GHz. The PA was excited by 40/200-MHz NR signals for communication mode, 100/500-MHz frequency-modulated continuous-wave (FMCW) signals for sensing mode, and a CW signal for power transfer mode. The test demonstrates that the proposed method significantly improves transmission performance while maintaining similar complexity.**

***Index Terms*— Digital predistortion (DPD), dynamic effects, integrated communication sensing and power transfer (ICSPT), neural network (NN), power amplifiers (PAs).**

Manuscript received 30 June 2024; revised 18 August 2024; accepted 22 August 2024. Date of publication 12 September 2024; date of current version 7 January 2025. This work was supported by the National Key Research and Development Program of China under Grant 2022YFB2902403. This article is an expanded version from the 2024 IEEE MTT-S International Microwave Symposium (IMS), Washington, DC, USA, June 16–21, 2024 [DOI: 10.1109/IMS40175.2024.10600393]. *(Corresponding author: Chao Yu.)*

Yucheng Yu, Luqi Yu, Xiao-Wei Zhu, and Peng Chen are with the State Key Laboratory of Millimeter Waves, Southeast University, Nanjing 210096, China (e-mail: ycyu@seu.edu.cn; lqyu@seu.edu.cn; xwzhu@seu.edu.cn; pchen@seu.edu.cn).

Ruijia Liu is with the School of Electrical and Electronic Engineering, University College Dublin, Dublin 4, D04 V1W8 Ireland (e-mail: ruijia.liu@ucd.ie).

Chao Yu is with the State Key Laboratory of Millimeter Waves, Southeast University, Nanjing 210096, China, and also with the Purple Mountain Laboratories, Nanjing 211111, China (e-mail: chao.yu@seu.edu.cn).

Color versions of one or more figures in this article are available at https://doi.org/10.1109/TMTT.2024.3452555.

Digital Object Identifier 10.1109/TMTT.2024.3452555

## I. Introduction

DRIVEN by the increasing demand for efficient spectrum utilization, enhanced system performance, and the convergence of various technological trends, integrated sensing and communications (ISAC) has attracted considerable interest of many researchers [1]. Meanwhile, wireless power transfer (WPT) is emerging as a promising solution to address the energy shortage of low-power devices by enabling wireless charging [2]. Therefore, WPT is expected to be integrated into ISAC systems, creating the integrated communication, sensing, and power transfer (ICSPT) paradigm [3], [4]. This integration is anticipated to play a pivotal role in future 6G networks. In the ICSPT paradigm, communication, sensing, and power transfer modes can be scheduled on time-division multiplexing (TDM) [5]. Fig. 1 illustrates the scenario of time-division ICSPT (TD-ICSPT). In communication mode, the system transmits modulation signals at relatively lower power levels to ensure reliable information transmission. Conversely, in sensing and power transfer modes, the system transmits continuous-wave (CW) waveforms at high power levels to facilitate sensing and power transfer tasks.

Achieving integration gains in ICSPT scenarios involves sharing the same hardware resources for different operating modes. The power amplifier (PA), a core component of the RF transmitter, must be optimized to accommodate all modes, ensuring high efficiency and linearity. Digital predistortion (DPD) technology is commonly used to maintain the desired performance of the PA in communication mode [6], [7]. DPD compensates for nonlinear distortion by cascading an inverse model of the PA in the baseband to predistort the input signals. For better linearization performance, various accurate DPD models have been proposed, such as the memory polynomial (MP) model [8], generalized MP (GMP) model [9], dynamic deviation reduction (DDR) model [10], decomposition vector rotation (DVR) model [11], and several neural network (NN)-based models [12], [13], [14], [15], [16], [17].

However, in ICSPT scenarios, seamless switching between different modes introduces significant dynamic effects,

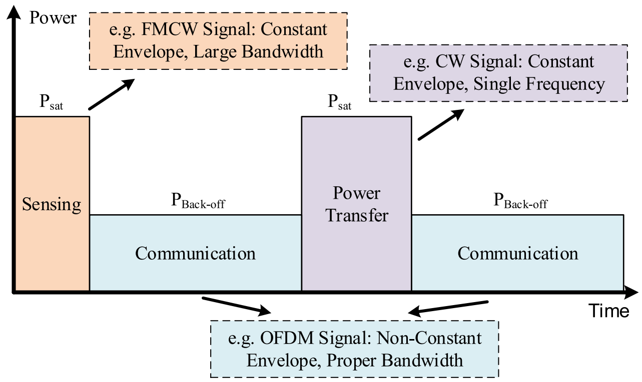


Fig. 1. TD-ICSPT scenario.

particularly in gallium nitride (GaN) PAs. During sensing or power transfer mode, the PA typically operates in a saturated state, while in communication mode, it operates at a back-off power level. This rapid and large range of power level changes during mode switching leads to significant thermal and trapping effects [18], [19]. In addition, fast-varying signal features, such as peak-to-average power ratio (PAPR) and bandwidth, introduce further dynamic characteristics, making PA's behavior more unpredictable. Consequently, the characteristics of the PA in the current operating mode are influenced by the previous operating mode and exhibit dynamic effects, which are challenging to linearize with conventional DPD models.

Some research efforts have addressed similar issues in conventional time-division duplex (TDD) scenarios. Tehrani et al. [20] use the average input power over a finite window as a metric for modeling long-term behavior changes. Barradas et al. [21] proposed using physics-based knowledge of transistors to calculate long-term memory vectors, which are then used to control model parameters. However, due to the limitations of conventional polynomial models, both the approaches assume a simple first-order dependence of the parameters on the long-term vectors, making it challenging to accurately capture complex dynamic effects. Besides, hybrid analog/digital linearization methods have been proposed for dealing with these issues [22], [23]. These methods primarily use an analog compensation circuit to control the gate–source bias voltage, compensating for gain variations caused by the electron trapping effect. A similar concept has been used to improve the pulse-to-pulse stability of pulsed radar [24]. However, analog circuits may lack accuracy and flexibility, especially in multistage or multitransistor PA architectures. Besides, these methods primarily focus on either communication or sensing modes individually, making them unsuitable for ICSPT scenarios. Therefore, a new model is required to accurately compensate for the distortion of PAs under ICSPT scenarios.

To address this issue, we previously explored dynamic effects in [25], developing a method for calculating dynamic state variables to track PA characteristic changes during mode switching. By injecting these variables into the NN model, we achieved accurate modeling of dynamic effects in communication mode. In this article, based on the behavioral modeling method reported in [25], we provide a more detailed analysis of dynamic state variables and introduce a novel method for calculating them. This new method uses 1-D-convolutional layers for efficient feature extraction and integrates with the subsequent NN model to further improve the performance. In addition, we extend the model to compensate for distortion in communication mode and in sensing and power transfer modes, maintaining proper complexity. Furthermore, we present comprehensive measurement results using 40/200-MHz NR signals for communication mode, 100/500-MHz frequency-modulated CW (FMCW) signals for sensing mode, and a CW signal for power transfer mode, tested on a millimeter-wave (mmWave) GaN two-stage Doherty PA. The results are compared with the existing methods to evaluate the effectiveness of our proposed approach.

The rest of this article is organized as follows. Section II details the method for calculating dynamic state variables. In Section III, the proposed DPD technique for the ICSPT scenario is elaborated. Section IV presents the experimental results conducted on the mmWave GaN Doherty PA. Finally, the article concludes in Section V.

## II. Dynamic State Variables' Calculation

### A. Dynamic State Variables

In TD-ICSPT scenarios, the operating power and characteristics of transmitted signals vary significantly among different modes. When mode switch occurs, the signal from the previous operating mode can affect the characteristics of the PA, causing PA's operating characteristics influenced by the long-term input signals. This can be expressed as

$$y(n) = f_{xy}(x(n), x(n-1), \dots, x(n-M_S), \dots, x(n-M_L)) \tag{1}$$

where $x(n)$ and $y(n)$ are the input and output signals of PA at instant $n$, respectively, and $M_S$, and $M_L$ are the short-time and long-time memory depths, respectively. $f_{xy}(\cdot)$ represents a nonlinear function from $x$ to $y$.

Given that the time constants of long-term behavior are significantly larger than those of short-term memory, $M_L$ is much larger than $M_S$. Using conventional DPD models to account for this dynamic effects would result in a prohibitively model size, making it impractical for communication systems.

From another point of view, the dynamic effects can be viewed as a slow change in the characteristics of the PA, managed by dynamic state variables $d(n)$. At instant $n$, the PA operates on a specific state determined by the long-term input signal, expressed as

$$d(n) = f_{xd}(x(n), x(n-1), \dots, x(n-M_L)) \tag{2}$$

where $f_{xd}(\cdot)$ represents a nonlinear function from $x$ to $d$.

In this approach, the long-term information at instant $n$ is summarized as dynamic state variables $d(n)$. Due to the slow influence of the dynamic effect, it can be separated from the short-term memory effect, as shown in Fig. 2; in this way, the output of the PA can be expressed as

$$y(n) = f_{xdy}(x(n), x(n-1), \dots, x(n-M_S), d(n)) \tag{3}$$

where $f_{xdd}(\cdot)$ represents a nonlinear function from $x$, $d$, to $y$.

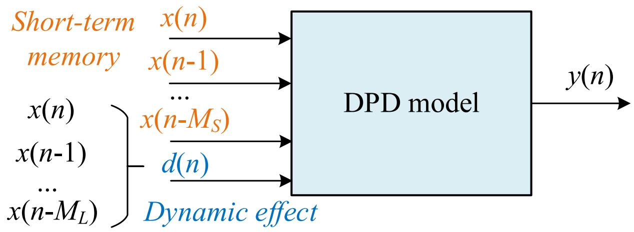


Fig. 2. Modeling dynamic effects through dynamic variables $d(n)$.

In this way, the model can be dramatically simplified. The main problem in compensating for dynamic effects lies in how to calculate suitable dynamic variables that can effectively characterize the long-term behavior of PAs.

### *B. Calculating Dynamic State Variables by Residual*

To address this issue, our preliminary work has proposed a method for calculating dynamic variables [25]. This approach calculates the dynamic variables through a recurrent method.

As a reasonable approximation, we assume that the dynamic state variables at the current instant $n$ depend only on the dynamic state variables at the previous instant $n-1$ and the current input signal $x(n)$

$$d(n) = f_{xdd}(x(n), d(n-1)) \tag{4}$$

where $f_{xdd}(\cdot)$ represents a nonlinear function to calculate the dynamic effects.

With this operation, the dynamic variables only depend on two input terms. However, it is still difficult to optimize since it has infinite memory length. To further simplify, we assume that $d(n-1)$ and $x(n)$ are independent and linearly related to $d(n)$. Besides, since the dynamic effects primarily depends on the power level of the input signal, $x(n)$ can be approximated as $|x(n)|$. Thus (4) can be simplified as

$$d(n) = c_1 \cdot |x(n)| + c_2 \cdot d(n-1) \tag{5}$$

where $c_1$ and $c_2$ are the parameters that control the updating rate of dynamic variables.

To prevent $d(n)$ from monotonously increasing or decreasing over time, we set $c_1 = 1-a$ and $c_2 = a$. Thus, we get

$$d(n) = (1-a) \cdot |x(n)| + a \cdot d(n-1) \tag{6}$$

where $a$ is the parameter controlling the updating rate of the dynamic state variables.

The dynamic variables' calculation block is shown in Fig. 3. After simplification, this expression has only one parameter and can be estimated using the residual-based method described in [21]. This method involves two steps.

The first step is to obtain the residuals resulting from long-term behavior. A memoryless model is used to capture input–output signals that include long-term behavior. The residuals, encompassing both short-term and long-term memory effects, are then low-pass-filtered. The filtered residuals represent the long-term behavioral residuals $R(n)$.

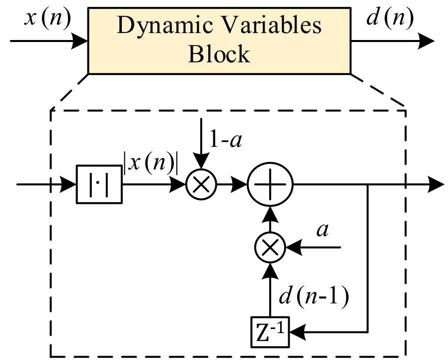


Fig. 3. Dynamic variables' block in [25].

The second step is to extract the parameter $a$ based on the residuals and (6). A nonlinear fitting method is used to minimize the error of the following equation:

$$\sum_n |R(n) - kd(n) - C|^2 \tag{7}$$

where $k$ is the linear factor, and $C$ is the bias.

The fitting process aims to find the best match of the dynamic variables with the long-term residuals, thus making sure the dynamic variables can represent the dynamic effects well. Since $d(n)$ shows an infinite memory length, it is difficult to be optimized with the NN model together. Once $d(n)$ is determined, the subsequent NN model can start training.

### *C. Calculating Dynamic State Variables Using NNs*

Although the above method was proved to be effective in [25], it has two limitations. First, it simplifies the calculating process of dynamic state variables, which neglect nonlinearities. Second, it separates the calculating of dynamic states from the calculating of final output signals, potentially yielding only locally optimal results and reducing final performance. Therefore, this article proposes a method for integrating the calculation of dynamic variables into the NN.

Revisiting (5), using the activation function $\phi(\cdot)$ at instant $n$ to introduce nonlinearity, to avoid infinite memory depth, truncated at moment $n - M_L$, expanding (5) as follows:

$$\begin{aligned} d(n) &= \phi(c_1 \cdot |x(n)| + c_2 \cdot d(n-1)) \\ &= \phi\big(c_1 \cdot |x(n)| + c_1 c_2 \cdot |x(n-1)| + c_2^2 \cdot d(n-2)\big) \\ &= \phi\big(c_1 \cdot |x(n)| + c_1 c_2 \cdot |x(n-1)| + c_1 c_2^2 \cdot |x(n-2)| \\ &\qquad + c_2^3 \cdot d(n-3)\big) \\ &= \phi\big(c_1 \cdot |x(n)| + c_1 c_2 \cdot |x(n-1)| + c_1 c_2^2 \cdot |x(n-2)| \\ &\qquad + c_1 c_2^3 \cdot |x(n-3)| + \cdots + c_1 c_2^{M_L} \cdot |x(n-M_L)|\big). \end{aligned} \tag{8}$$

This shows that $d(n)$ is related to each input signal from time step $n - M_L$ to time step $n$ with an independent coefficient. Using a multilayer perceptron (MLP) to calculate the dynamic variables would require assigning a coefficient to each moment, significantly increasing the number of parameters since MLP cannot leverage the prior relationship

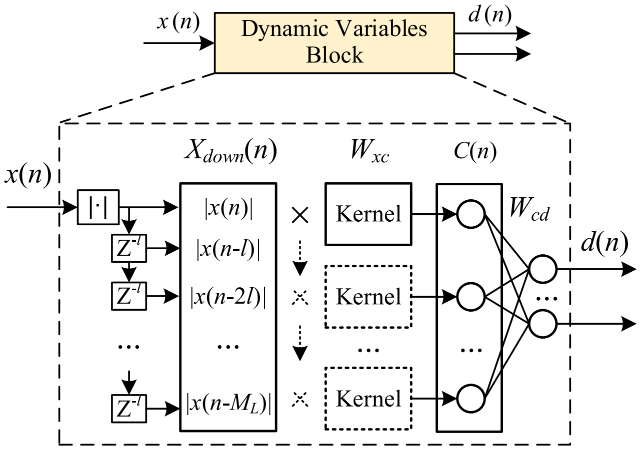


Fig. 4. Dynamic variables' block using 1D-CNN.

between coefficients. Further examination reveals that the coefficients for earlier time steps must be multiplied by an additional $c_2$ compared with the next time step, which is the same in every time step, indicating a translation invariance property. This suggests using recurrent NNs (RNNs) or 1-D-convolutional NNs (1D-CNNs) to exploit this property. Comparing these two models, RNNs calculate hidden states recurrently, which offers higher parameter utilization but requires backpropagation through time (BPTT) for training the model, making them prone to issues such as gradient explosion. While methods such as Just Another NETwork (JANET) or Echo State Networks can alleviate some of these challenges, their training complexity remains higher than that of feedforward NNs. Furthermore, RNNs can suffer from redundancy and delay problems due to recurrent connections in the hidden layer while model running [26], [27]. Besides, the 1D-CNN uses feedforward architecture for feature extraction, which has higher training and running efficiency. Therefore, 1D-CNN is chosen for the dynamic variables' block.

The dynamic variables' block using 1-D-convolutional layer is illustrated in Fig. 4. The input sequence and the convolution kernel generate the output through a mutual correlation operation. The convolution kernel is then translated with a specific stride and computed again until the entire input sequence is covered. After the convolution operation, the output signal can be expressed as

$$\begin{aligned} C(n) &= X(n) \otimes W_{xc} \\ &= [|(x(n)|, |x(n-1)|, |x(n-2)|, \ldots, |x(n-M_L)|)] \\ &\quad \otimes W_{xc} \end{aligned} \tag{9}$$

where $C(n)$ is the output of the convolutional layer, $X(n)$ is the long-term input sequence, $W_{xc}$ is the weights in the convolution weights, and $\otimes$ is the convolutional operation.

While the using of 1D-CNN reduces the number of coefficients, it does not reduce running complexity, such as the floating point operations (FLOPs). To address this, a downsampling approach can be used to reduce the number of samples of the input long-term signal. After downsampling, the convolutional layer operation can be expressed as

$$\begin{aligned} C(n) &= X_{\text{down}}(n) \otimes W_{xc} \\ &= [(|x(n)|, |x(n-l)|, |x(n-2l)|, \ldots, |x(n-M_L)|)] \\ &\quad \otimes W_{xc} \end{aligned} \tag{10}$$

where $l$ is the downsampling rate. With this operation, the running complexity can be significantly reduced.

The output of the 1-D-convolutional layer is then passed through a fully connected layer to obtain the dynamic variables. This layer also uses nonlinear activation functions to further process the extracted dynamic features. The output of the fully connected layer can be expressed as

$$d(n) = \phi(C(n)W_{\text{cd}} + b) \tag{11}$$

where $W_{\text{cd}}$ is the weight of the fully connected layer, and $b$ is the bias. The number of dynamic variables can be adjusted by modifying the number of neurons in the fully connected layer. Multiple dynamic variables can track various changes in the PA operating state. Although these variables share a similar calculation structure, subtle differences in their weights allow them to focus on different time segments of the input signal, thereby capturing different time constants of long-term effects. It is important to note that the dynamic behavior of GaN PAs may be influenced by multiple factors with varying time constants, making multiple dynamic variables crucial for effectively compensating for dynamic effects.

These dynamic state variables $d(n)$ can be injected into the subsequent NN to contribute to the output signal. Unlike the previous extraction method, the training of $d(n)$ uses the NN structure, which can be optimized together with the subsequent model to extract more appropriate dynamic states, thereby improving modeling performance.

## III. DPD Technique for ICSPT Application

### A. DPD Model for Communication Mode

In communication mode, the DPD model must address both the dynamic effects and the inherent short-term memory effects and nonlinearities of the PA. This can be achieved using an NN-based DPD model to realize (3). It is worth mentioning that almost any NN behavioral model can achieve this by simply injecting dynamic variables into its input layer.

To reduce the complexity of the model, in our previous work we separated the dynamic effects from PA's common short-term properties [25], and the model has two parts, as shown in Fig. 5. The upper part of the model addresses the common behavior of the PA, which are predictable and independent of dynamic variables. Here, a simple polynomial model suffices to represent these characteristics accurately.

The lower part of the model specifically targets the dynamic effects. This box uses an NN, known for its powerful fitting capabilities, to track and model changes caused by dynamic influences. By leveraging the ability of the NN model to learn and generalize from data, we can accurately capture the complex nonlinearity associated with the dynamic effects of the PA.

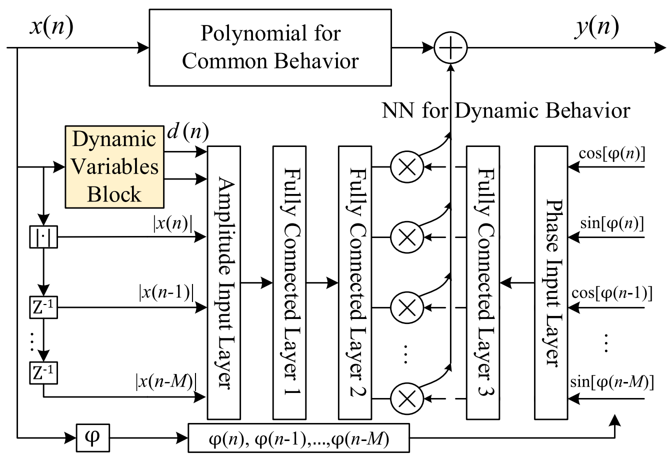


Fig. 5. Proposed DPD model of the communication mode.

The dynamic variables are injected into the input layer alongside the amplitude of the input signal. The input vector $\boldsymbol{x}_a(n)$ can be expressed as

$$\boldsymbol{x}_a(n) = [|x(n)|, \dots, |x(n - M_s)|, d(n)]. \tag{12}$$

After the input layer, several fully connected layers characterize the amplitude nonlinearity. The output from these layers includes nonlinear features extracted from the input signal and dynamic variable, preparing the data for further phase recovery.

Dynamic effects can also induce phase deviations. To address this, we incorporate a fully connected layer for phase preprocessing, aimed at compensating for possible phase distortion and enhancing phase recovery accuracy. The input vector of the phase processing part $\boldsymbol{x}_p(n)$ consists of the cosine and sine values of the input signal phase

$$\boldsymbol{x}_p(n) = [\cos[\varphi(n)], \sin[\varphi(n)], \dots, \sin[\varphi(n - M_s)] \tag{13}$$

where $\varphi(n)$ is the phase of the input signal at instant $n$.

The fully connected layer applies appropriate weightings and transformations to the input phase data, learning and capturing the nonlinear relationships associated with phase deviations. The extracted phase information is then used for phase recovery [13]. The output of the NN block $y_{nn}(n)$ can be expressed as

$$y_{nn}(n) = f_a(\boldsymbol{x}_a) \cdot f_p(\boldsymbol{x}_p) \tag{14}$$

where $f_a(\cdot)$ and $f_p(\cdot)$ are the nonlinear functions of the amplitude part and phase part, respectively. This process combines nonlinear features from the amplitude processing part with the processed phase information, reconstructing a more accurate representation of the output signal that accounts for both the amplitude and phase characteristics affected by dynamic effects.

The output of the NN block is merged with the polynomial block to obtain the final output signal. The entire model for the communication mode is built within an NN framework, allowing all the weights to be optimized together using NN optimization algorithms.

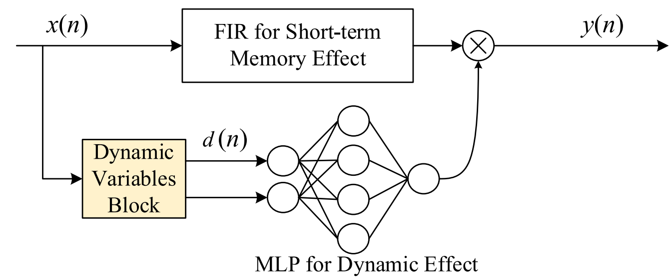


Fig. 6. Proposed DPD model of the sensing and power transfer modes.

By incorporating the dynamic variables into the model, we effectively account for the influence of the long-term input signal. This enables the NN to use its strong fitting capabilities to compensate for dynamic effects in ICSPT scenarios.

### *B. DPD Model for Sensing and Power Transfer Modes*

Although sensing and power transfer modes are generally less sensitive to the distortion of PA, certain scenarios, such as moving target indication (MTI) [28], phase-attached radar communications (PARC) [29], and scenarios requiring highly stable power transfer, also demand high accuracy in signal transmission. Therefore, it is crucial to consider distortion compensation in these modes.

Unlike communication modes, sensing and power transfer modes typically use constant-envelope signals, such as FMCW waveforms for sensing mode and CW waveforms for power transfer mode. For these signals, nonlinear characteristics do not cause distortion, but memory effects can still affect stability.

The compensation model is shown in Fig. 6. To address short-term memory effects, a simple finite impulse response (FIR) filter can be used. The output signal of the FIR filter $y_{\mathrm{FIR}}(n)$ can be expressed as

$$y_{\mathrm{FIR}}(n) = \sum_{m=0}^{M_s} (a_m \cdot x(n - m)) \tag{15}$$

where $a_m$ is the coefficient of the FIR filter.

Dynamic effects can be seen as gradual changes in PA gain for constant-envelope signals [24]. Compensation for these effects involves capturing the relationship between dynamic state variables and gain changes through an MLP. This relationship is then used to adjust the output of the FIR filter

$$y_{\mathrm{spt}}(n) = y_{\mathrm{FIR}}(n) \cdot F_{\mathrm{MLP}}(d(n)) \tag{16}$$

where $y_{\mathrm{spt}}(n)$ is the compensated signal of the sensing or power transfer mode in the ICSPT scenario, and $F_{\mathrm{MLP}}(\cdot)$ is the function of MLP model.

In this way, the gain dynamics in the sense and power transfer modes due to the dynamic effects can be compensated by adjusting the amplitude of the input signal, thus ensuring the performance stability of the sense and power transfer modes in the TD-ICSPT scenarios.

### C. Training of the Proposed Model

Before the system operates, the model requires offline training. Initially, a training dataset must be obtained. Since training is conducted offline, ideal DPD signals for the TD-ICSPT waveform can be generated using iterative learning control (ILC) [30]. The input and ideal DPD signals are then separated into communication, sensing and power transfer modes. Given the complex nonlinear characteristics of the communication mode, the compensation model for this mode is trained first. After training, the coefficients for both the communication model and the dynamic variables block are determined together. The dynamic variables' block is then fixed, and the coefficients for the sensing and power transfer model are trained using data from these respective modes. The training algorithm is summarized as Algorithm 1. Once both the models are trained, the entire ICSPT compensation model is ready for operation.

**Algorithm 1** Training of the ICSPT DPD Model

**Input**: TD-ICSPT input signal $x$, TD-ICSPT ideal DPD signal $u$

**Output**: Trained ICSPT DPD model

1: Split the TD signal into: communication signal: $x_{com}$, $u_{com}$, sensing and power transfer mode signal: $x_{spt}$, $u_{spt}$

2: Train the model for communication mode using $x_{com}$, $u_{com}$

3: Determine the model coefficients of the communication mode and the dynamic variables' block

4: Fixe the coefficients of dynamic variables' block, train the model for the sensing and power transfer mode

5: Determine the model coefficients of the sensing and power transfer mode using $x_{spt}$, $u_{spt}$.

During real-time deployment, the characteristics of PA may change due to unpredicted factors. In such cases, the coefficients of the model can be updated using lower complexity methods, such as continual learning [31] or direct learning (DLA)-based fine-tuning [16], ensuring the model remains effective over time. The complexity of these updating methods can be comparable to that of polynomial-based models.

### D. System Running

The proposed ICSPT DPD system integrates the compensation models for different operating modes while sharing the same dynamic variables' block. In communication mode, the input signals and outputs from the dynamic variables block feed into the communication mode model to produce the predistorted signal, ensuring communication quality. In sensing and power transfer modes, the input signal and dynamic variables connect to the respective mode's model to compensate for PA gain bias caused by dynamic effects. This approach introduces minimal additional complexity for sensing and power transfer modes while maintaining overall linearization performance. With simple switching, the model can linearize the communication mode, as well as compensate for the distortion in sensing and power transfer modes, with appropriate complexity.

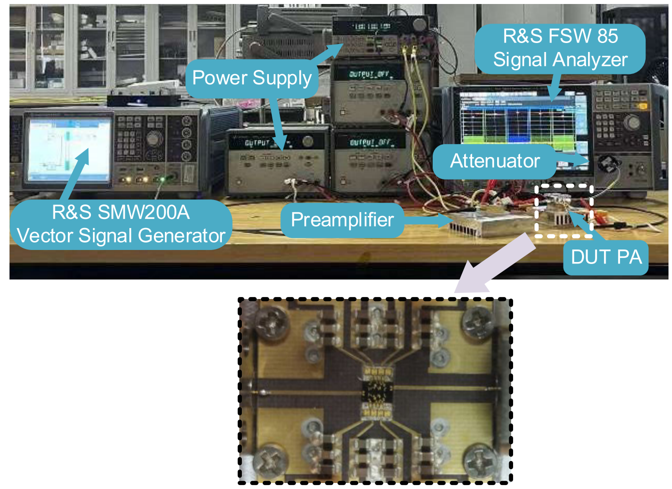


Fig. 7. Testbench setup.

TABLE I
SIGNAL CONFIGURATIONS OF THE ICSPT SIGNAL

| Mode | Signal Type | Bandwidth | PAPR |
|---|---|---|---|
| Communication | 5G NR | 40/200 MHz | 9.5 dB |
| Sensing | FMCW | 100/500 MHz | N/A |
| Power Transfer | CW | N/A | N/A |

## IV. MEASUREMENT RESULTS

### A. Experimental Setup and Configurations

To validate the proposed method, a testbench was set as shown in Fig. 7. The device under test (DUT) is an in-house designed mmWave two-stage GaN microwave monolithic integrated circuit (MMIC) Doherty PA, operated at 24–28 GHz with a measured saturated output power of 35.5 dBm. In sensing and power transfer modes, the operating power is around 35.5 dBm, while the average power in communications mode is approximately 26 dBm. The drain power supplies for all the transistors are set to 20 V. The PA has a saturated power density of 0.59 W/mm$^2$ and a size of 2.99 $\times$ 1.99 mm. Further detailed information can be found in [32]. During the experiment, the baseband test signal is downloaded from the PC and upconverted to mmWave around 27 GHz by the vector signal generator (SMW200A). After passing through a preamplifier, the signal is injected into the DUT. The vector signal analyzer (FSW85) captures the output signal after attenuation and sends it back to the PC for signal processing. During the test, 1/4 data were used for training the model, while the rest 3/4 were used for validation.

The TD-ICSPT test signal is composed of three components: a 5G NR signal for communication mode, an FMCW signal for sensing mode, and a CW signal for power transfer mode, and the signal configuration is shown in Table I. Tests were conducted at various signal bandwidths, including 40-MHz 5G NR and 100-MHz FMCW signals, as well as wider bandwidths of 200-MHz 5G NR and 500-MHz FMCW signals. The sampling rates were set to 200 MHz and 1 GHz, respectively. In both the tests, the carrier frequency was set to 27 GHz.

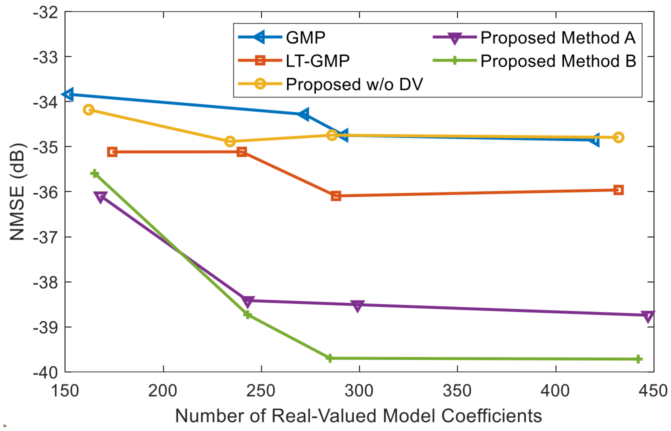


Fig. 8. NMSE of the compared models with different numbers of real-valued model coefficients for the 40-MHz 5G NR signal.

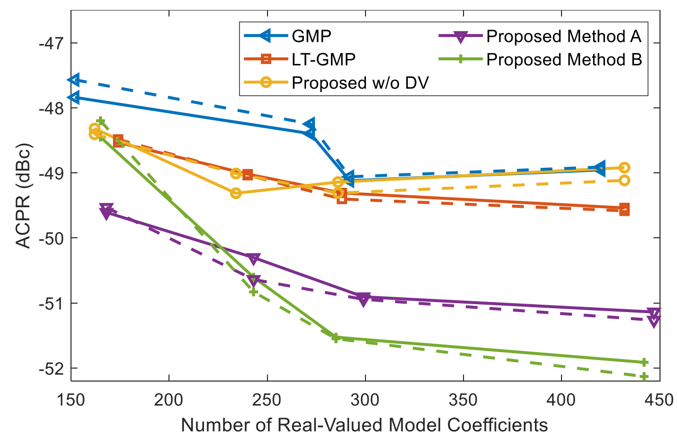


Fig. 9. ACPR of the compared models with different numbers of real-valued model coefficients for the 40-MHz 5G NR signal (solid line: left band, dotted line: right band).

To verify the effectiveness of the proposed method in communication mode, several DPD models are compared: 1) GMP model [9]; 2) LT-GMP model: the GMP model with long-term memory compensation [21]; 3) proposed model w/o DV: proposed model without the integration of dynamic variables $d(n)$; 4) proposed method A: the proposed model with the dynamic variables block from our previous work [25]; and 5) proposed method B: the proposed model with the dynamic variables block in this article, using one 1-D-convolution kernel with a size of 10, a stride of 10, the input sequence length is set as 100 after downsampling, and the downsampling rate is set as 100 and 500 for 200-MHz and 1-GHz sampling rate, respectively. For the sensing and power transfer mode, the proposed method is compared with the FIR model.

The normalized mean square error (NMSE), adjacent channel power ratio (ACPR), and error vector magnitude (EVM) are used to assess modeling performance, while the number of real-valued coefficients and FLOPs [33] are used to quantify the complexity, and the complex-valued coefficients are counted as two real-valued coefficients for comparison.

### B. Test With 40-MHz 5G NR and 100-MHz FMCW Signals

The experimental validation began with testing a 40-MHz 5G NR signal and a 100-MHz FMCW signal. To evaluate the performance of different models across varying levels of complexity, a series of configurations were selected for each model to measure linearization performance in communication mode.

During testing, the number of real coefficients for each model was incremented from around 150 until performance plateaued. For the proposed NN model, the number of neurons was varied from 3 to 12. For the proposed method B, the number of dynamic variables ranged from 1 to 3. The configurations for the GMP and LT-GMP models were optimized to achieve their best performance at each evaluation point. Figs. 8 and 9 display the NMSE and ACPR performance of different models at various numbers of real-valued model coefficients.

As shown in Fig. 8, the GMP model performs poorly due to it does not consider the dynamic effect, and continuing to increase coefficients does not enhance performance. The LT-GMP model shows better performance but hits a bottleneck at around −36 dB. The proposed method A significantly improves linearization performance, achieving levels below −38 dB, while the proposed model without dynamic variables performs similar to the GMP model. This indicates that dynamic variables are crucial for compensating dynamic effects. Compared with the proposed method A, the proposed method B exhibits suboptimal performance with fewer coefficients due to the added complexity of the dynamic variables' block, which hampers the NN's nonlinear fitting ability. However, with more coefficients, the performance of the proposed method B improves significantly, showing higher performance potential than the proposed method A, indicating the effectiveness of the dynamic variables block. The configuration of the proposed method B with the lowest complexity used one dynamic variable, the highest complexity used three dynamic variables, and the middle configurations used two dynamic variables. The experimental results show that the proposed method B achieves a better performance–complexity tradeoff with two dynamic variables.

TABLE II
PERFORMANCE COMPARISON FOR THE 40-MHz 5G NR SIGNAL

| Model | NMSE (dB) | ACPR (dBc) | EVM | No. of real-valued coefficients | FLOPs |
|---|---|---|---|---|---|
| w/o DPD | -18.4 | -27.3/-27.1 | 10.63 % | N/A | N/A |
| GMP | -34.7 | -49.1/-49.1 | 1.74 % | 292 | 1166 |
| LT-GMP | -36.1 | -49.3/-49.4 | 1.64 % | 288 | 1150 |
| Proposed w/o DV | -34.7 | -49.1/-49.3 | 1.80 % | 286 | 554 |
| Proposed Method A | -38.5 | -50.9/-50.9 | 1.31 % | 299 | 580 |
| Proposed Method B | -39.7 | -51.5/-51.5 | 1.15 % | 285 | 752 |

To provide a detailed comparison, we limited the number of coefficients of the different models to a similar range and evaluated their performance. In this test, the number of real-valued coefficients was set to around 300. The detailed results are shown in Table II. In this case, the GMP model configurations are $K_a = 9$, $L_a = 4$, $K_b = 4$, $L_b = 3$,

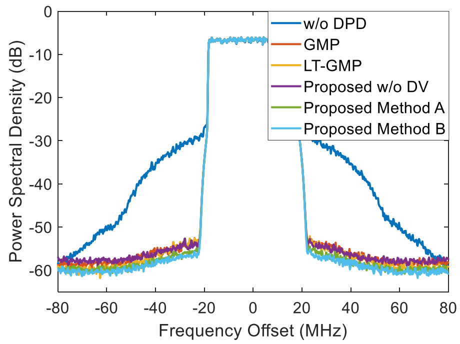


Fig. 10. PSD results of the 40-MHz NR signal.

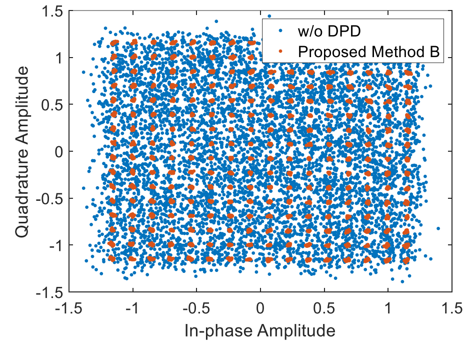


Fig. 11. Demodulation of the 40-MHz NR signal.

$M_b = 3$, $K_c = 4$, $L_c = 3$, and $M_c = 3$. The LT-GMP model configurations are $K_a = 8$, $L_a = 3$, $K_b = 2$, $L_b = 2$, $M_b = 1$, $K_c = 2$, $L_c = 2$, and $M_c = 1$, with the two auxiliary branches having the same parameters as the main branch. For the proposed model, the polynomial block uses the MP model [8] with the parameters set as $K = 4$, $L = 3$. The neurons of the fully connected layers of the NN block are set as [13,9,6] for the proposed model w/o DV and proposed method A. For the proposed method B, it is set as [9,9,6].

Table II confirms that the proposed method performs well with a similar number of real-valued coefficients. Both the proposed methods outperform LT-GMP by at least 2 dB in NMSE and 1.5 dB in ACPR. When comparing the two proposed methods, the proposed method B shows a 1.2-dB improvement in NMSE and a 0.6-dB improvement in ACPR, further proving the effectiveness of the proposed dynamic variables' block. Due to the introduction of 1D-CNN, the proposed method B demonstrates more FLOPs than the proposed method A for similar coefficients. However, when the FLOPs of the two methods are controlled at similar values, the proposed method B still has a performance advantage. We also measured the model running time using MATLAB's tic-toc functions. All the methods took about 0.4 s to process 80 000 samples of DPD signals. It is important to note that the computation time measured in MATLAB may differ from the actual time in a real system. Depending on hardware implementation, resource usage may vary between models. However, these results indicate that the proposed method is capable of real-time operation. The power spectral density comparison between the models is shown in Fig. 10, and the demodulation results for the proposed method B are shown in Fig. 11.

For sensing and power transfer modes, distortion compensation performance was evaluated using NMSE. The memory depth of the FIR model is set as 5, while the hidden neuron of the MLP is set as 5. The result is shown in Table III. It can be seen that the proposed model performs significantly better than the FIR model. Despite the low complexity of the FIR model, increasing the complexity does not change its performance due to its inability to account for dynamic effects' compensation. It is worth noting that the main complexity of the proposed method is caused by the dynamic variables block, and since it is shared with the communication modes, the complete ICSPT DPD system does not introduce a significant amount of additional complexity due to the consideration of the sensing and power transfer modes. Fig. 12 shows the output power offset of the sensing and power transfer mode signal after FIR model compensation and after proposed method compensation. Obviously, the FIR model fails to compensate the gain offset due to dynamic effects, the gain fluctuations around 0.5 dB, while the proposed method reduces to 0.15 dB, indicating its effectiveness in the sensing and power transfer mode.

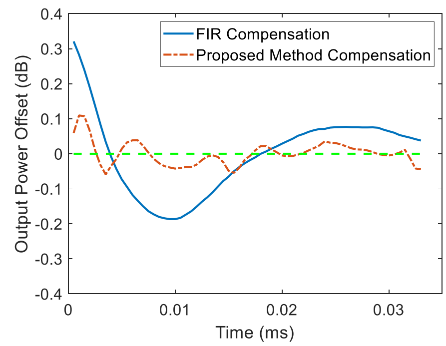


Fig. 12. Output power offset of CW signal at 200-MHz sampling rate.

TABLE III
PERFORMANCE COMPARISON FOR 100-MHz FMCW SIGNAL AND CW SIGNALS

| Model | NMSE (dB) | No. of real-valued coefficients | FLOPs |
|---|---|---|---|
| w/o DPD | -29.3 | N/A | N/A |
| FIR | -32.6 | 12 | 46 |
| Proposed Method | -35.8 | 66 | 344 |

To comprehensively assess the entire proposed ICSPT compensation model, a comparative analysis was conducted with conventional compensation schemes. The results, shown in Fig. 13, indicate that the FIR and GMP models are unable to compensate for dynamic effects, resulting in performance deterioration near mode switching. Using the LT-GMP model instead of the GMP model improves the performance of communication mode, but performance degradation during mode switching remains. It should be noted that the proposed method continues to outperform other methods even after long periods when the long-term effects of other operating modes have diminished. This is because the GMP model lacks the

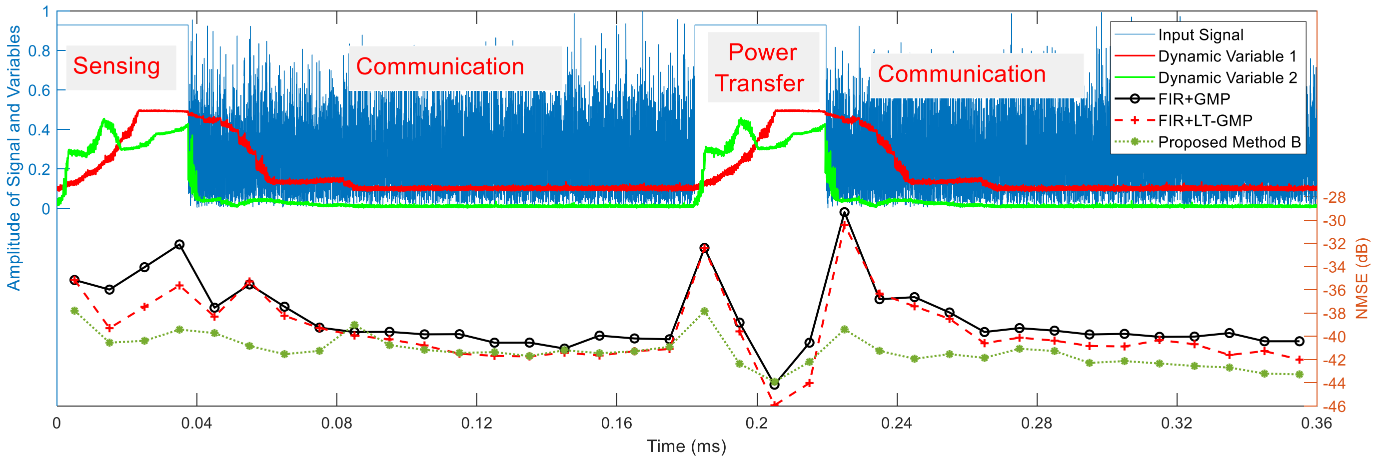


Fig. 13. Test results of 40-MHz 5G NR and 100-MHz FMCW signals: amplitude of the input TD-ICSPT signal and dynamic variables (left axis), and comparison of model performance versus time (right axis).

ability to effectively model long-term effects, necessitating a tradeoff between long-term memory effects and normal DPD, which reduces DPD performance under normal conditions. Similarly, although the LT-GMP model uses long-term auxiliary branches to address long-term memory effects, it only considers first-order dependence on long-term vectors, limiting its ability to fully compensate for these effects. As a result, its performance fails to match the proposed method over time.

The trend of dynamic variables in the proposed method B is also shown in Fig. 13. It can be seen that the dynamic variables change when the operating modes' switch occurs, but they exhibit different trends and time constants, making them more effective in compensating for dynamic effects in ICSPT scenarios. The proposed method demonstrates superior performance across communication, sensing, and power transfer modes, confirming its effectiveness.

### C. Test With 200-MHz 5G NR and 500-MHz FMCW Signals

To evaluate the proposed method on wider bandwidths, we conducted experimental validation on 200-MHz 5G NR and 500-MHz FMCW signals.

Similar to Section IV-B, we assessed the performance of different models with varying numbers of real-valued coefficients. The number of real-valued coefficients for each model was incremented from around 250 until performance ceased to improve. For the NN models, the number of neurons was varied from 5 to 25. The GMP and LT-GMP models were tuned for best performance at each complexity level. Figs. 14 and 15 show the NMSE and ACPR performance of different models.

It can be observed from Figs. 14 and 15 that the GMP and LT-GMP models still fail to achieve satisfactory DPD performance. The proposed model without dynamic variables performs only slightly better than the GMP model. However, when dynamic variables are calculated and injected into the model, the proposed method shows significant performance improvement. In addition, the proposed method B outperforms the proposed method A, illustrating the effectiveness of the proposed dynamic variables' block.

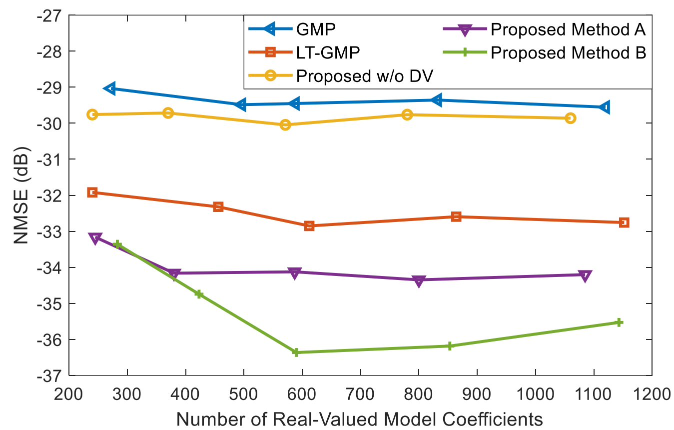


Fig. 14. NMSE of the compared models with different numbers of real-valued model coefficients for the 200-MHz 5G NR signal.

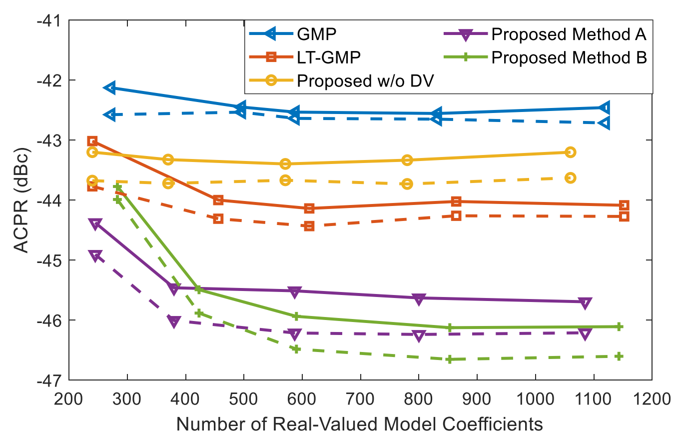


Fig. 15. ACPR of the compared models with different numbers of real-valued model coefficients for the 200-MHz 5G NR signal (solid line: left band, dotted line: right band).

For a detailed comparison, we limited the complexity of each model to around 600 real-valued coefficients. The results are shown in Table IV. In this case, the GMP model configurations are $K_a = 8$, $L_a = 5$, $K_b = 5$, $L_b = 5$, $M_b = 4$, $K_c = 5$, $L_c = 5$, and $M_c = 4$. The LT-GMP

TABLE IV
PERFORMANCE COMPARISON FOR THE 200-MHz 5G NR SIGNAL

| Model | NMSE (dB) | ACPR (dBc) | EVM | No. of real-valued coefficients | FLOPs |
|---|---|---|---|---|---|
| w/o DPD | -18.1 | -27.6/-27.1 | 10.44 % | N/A | N/A |
| GMP | -29.5 | -42.5/-42.6 | 3.14 % | 588 | 2350 |
| LT-GMP | -32.9 | -44.1/-44.4 | 2.52 % | 612 | 2446 |
| Proposed w/o DV | -29.7 | -43.3/-43.7 | 2.83 % | 571 | 1119 |
| Proposed Method A | -34.1 | -45.5/-46.2 | 1.90 % | 587 | 1151 |
| Proposed Method B | -36.4 | -45.9/-46.5 | 1.55 % | 590 | 1355 |

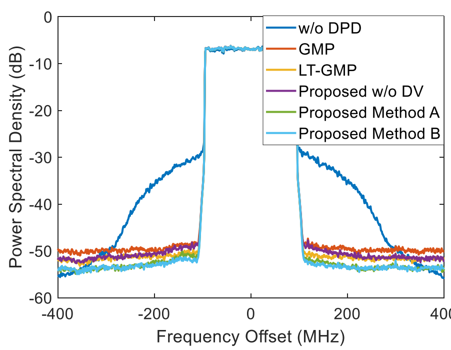


Fig. 16. PSD results of the 200-MHz NR signal.

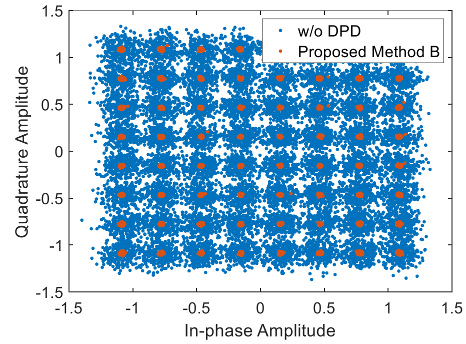


Fig. 17. Demodulation of the 200-MHz NR signal.

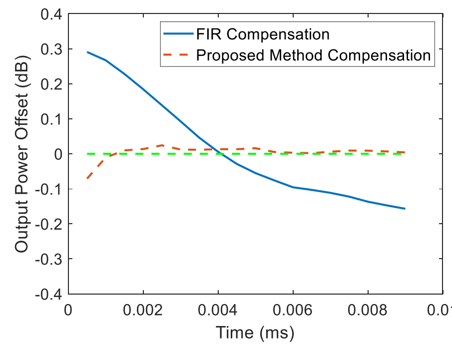


Fig. 18. Output power offset of CW signal at 1-GHz sampling rate.

TABLE V
PERFORMANCE COMPARISON FOR 500-MHz FMCW SIGNAL AND CW SIGNALS

| Model | NMSE (dB) | No. of real-valued coefficients | FLOPs |
|---|---|---|---|
| w/o DPD | -22.7 | N/A | N/A |
| FIR | -30.5 | 24 | 94 |
| Proposed Method | -35.0 | 78 | 392 |

model configurations are $K_a = 8$, $L_a = 5$, $K_b = 3$, $L_b = 3$, $M_b = 2$, $K_c = 3$, $L_c = 3$, and $M_c = 2$, with the auxiliary branches having the same parameters as the main branch. For the proposed model, the polynomial block uses the MP model [8] with the parameters set as $K = 4$ and $L = 5$. The neurons of the fully connected layers of the NN block are set as [16,15,10] for the proposed model w/o DV and the proposed method A. For the proposed method B, it is set as [15,15,10].

Table IV demonstrates that the proposed method outperforms conventional models. Both the proposed methods exceed LT-GMP by at least 1.2 dB in NMSE and 1.5 dB in ACPR. Comparing the two proposed methods, the proposed method B shows a 2.3-dB improvement in NMSE and a 0.4-dB improvement in ACPR, further proving the effectiveness. The power spectral density comparison between models is shown in Fig. 16, and the demodulation results of the proposed method B are shown in Fig. 17.

The results of sensing and power transfer modes are shown in Table V. The memory depth of the FIR model is set as 11, while the hidden neuron of the MLP is set as 5. The proposed model performs significantly better than the FIR model. Fig. 18 shows the output power offset of the sensing and power transfer mode after the FIR model and proposed method compensation. Due to the enhancement of the signal bandwidth, the sensing mode uses a shorter time to send the complete signal. It can be seen that the output signal power exhibits a large offset after compensation by the FIR model throughout the signal duration, whereas the proposed method still can achieve effective compensation and reduce the output power fluctuations to around 0.1 dB.

Finally, the proposed ICSPT compensation model was compared with conventional compensation schemes. The results are shown in Fig. 19. Conventional schemes experience performance deterioration when switching modes. However, the proposed method can effectively compensate for this dynamic effect. The trend of the dynamic variables is shown in Fig. 19. As observed, the trends differ slightly from those in Fig. 13. This variation occurs because, in NN-based models, the primary function of dynamic variables is to differentiate the distinct impacts of dynamic effects on PA states. The dynamic variables in both Figs. 13 and 19 can perform this task effectively.

It is worth noting that in the broadband test, the shorter duration of the communication mode increases the proportion of signals affected by long-term memory effects. This forces the normal DPD to compromise even more to compensate for these effects, widening the performance gap between other DPD methods and the proposed method. The results of the experiment demonstrated similar conclusions to the test in

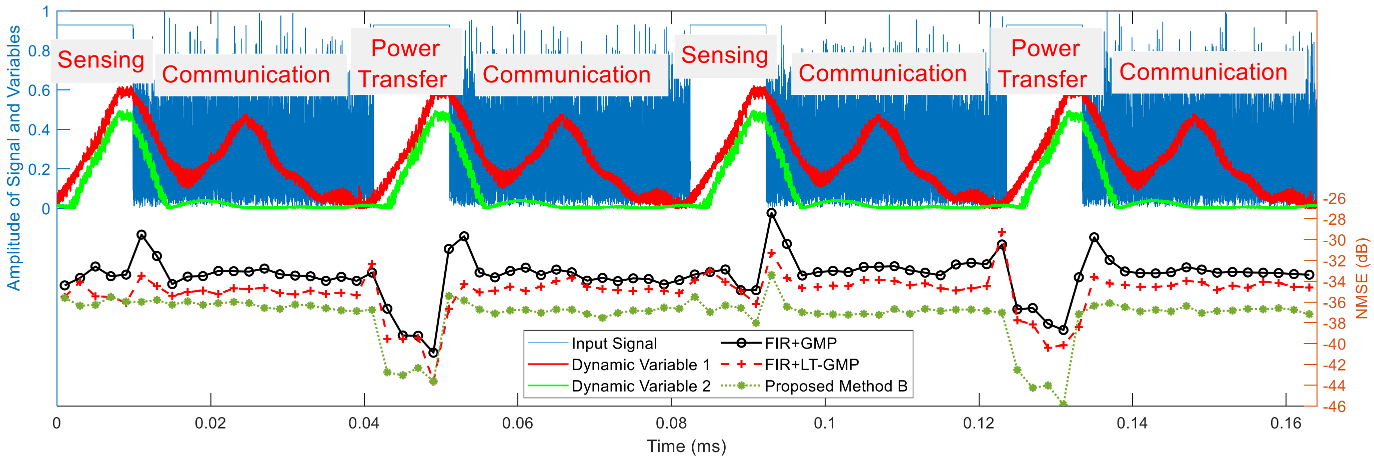


Fig. 19. Test results of 200-MHz 5G NR and 500-MHz FMCW signals: amplitude of the input TD-ICSPT signal and dynamic variables (left axis), and comparison of model performance versus time (right axis).

Section IV-B, which indicates that the proposed method is still effective in more complex transmission scenarios.

## V. Conclusion

In this article, we propose a novel distortion compensation model for the linearization of PAs in 6G ICSPT scenarios. By introducing dynamic variables, we effectively capture the changes in PA characteristics during mode switching with low complexity. The carefully designed dynamic variable calculation block enhances this capability. Furthermore, we developed specific compensation models for communication, sensing, and power transfer modes within the ICSPT framework, ensuring that distortion compensation is achieved with appropriate complexity for each mode. The experimental results on a mmWave GaN Doherty PA demonstrate that our proposed method significantly outperforms the existing schemes, highlighting its potential as a promising solution for future ICSPT scenarios.

## References

[1] F. Liu et al., "Integrated sensing and communications: Toward dual-functional wireless networks for 6G and beyond," *IEEE J. Sel. Areas Commun.*, vol. 40, no. 6, pp. 1728–1767, Jun. 2022.

[2] Y. Zeng, B. Clerckx, and R. Zhang, "Communications and signals design for wireless power transmission," *IEEE Trans. Commun.*, vol. 65, no. 5, pp. 2264–2290, May 2017.

[3] Y. Yang, H. Gao, X. Yang, R. Cao, and Y. Fan, "Joint beamforming for RIS-assisted integrated communication, sensing and power transfer systems," *IEEE Wireless Commun. Lett.*, vol. 13, no. 2, pp. 288–292, Feb. 2024.

[4] X. Li, X. Yi, Z. Zhou, K. Han, Z. Han, and Y. Gong, "Multi-user beamforming design for integrating sensing, communications, and power transfer," in *Proc. IEEE Wireless Commun. Netw. Conf. (WCNC)*, Mar. 2023, pp. 1–6.

[5] Q. Zhang, H. Sun, X. Gao, X. Wang, and Z. Feng, "Time-division ISAC enabled connected automated vehicles cooperation algorithm design and performance evaluation," *IEEE J. Sel. Areas Commun.*, vol. 40, no. 7, pp. 2206–2218, Jul. 2022.

[6] F. M. Ghannouchi and O. Hammi, "Behavioral modeling and predistortion," *IEEE Microw. Mag.*, vol. 10, no. 7, pp. 52–64, Dec. 2009.

[7] L. Guan and A. Zhu, "Green communications: Digital predistortion for wideband RF power amplifiers," *IEEE Microw. Mag.*, vol. 15, no. 7, pp. 84–99, Nov. 2014.

[8] L. Ding et al., "A robust digital baseband predistorter constructed using memory polynomials," *IEEE Trans. Commun.*, vol. 52, no. 1, pp. 159–165, Jan. 2004.

[9] D. R. Morgan, Z. Ma, J. Kim, M. G. Zierdt, and J. Pastalan, "A generalized memory polynomial model for digital predistortion of RF power amplifiers," *IEEE Trans. Signal Process.*, vol. 54, no. 10, pp. 3852–3860, Oct. 2006.

[10] A. Zhu, J. C. Pedro, and T. J. Brazil, "Dynamic deviation reduction-based Volterra behavioral modeling of RF power amplifiers," *IEEE Trans. Microw. Theory Techn.*, vol. 54, no. 12, pp. 4323–4332, Dec. 2006.

[11] A. Zhu, "Decomposed vector rotation-based behavioral modeling for digital predistortion of RF power amplifiers," *IEEE Trans. Microw. Theory Techn.*, vol. 63, no. 2, pp. 737–744, Feb. 2015.

[12] T. Liu, S. Boumaiza, and F. M. Ghannouchi, "Dynamic behavioral modeling of 3G power amplifiers using real-valued time-delay neural networks," *IEEE Trans. Microw. Theory Techn.*, vol. 52, no. 3, pp. 1025–1033, Mar. 2004.

[13] Y. Zhang, Y. Li, F. Liu, and A. Zhu, "Vector decomposition based time-delay neural network behavioral model for digital predistortion of RF power amplifiers," *IEEE Access*, vol. 7, pp. 91559–91568, 2019.

[14] A. Fischer-Bühner, L. Anttila, M. D. Gomony, and M. Valkama, "Phase-normalized neural network for linearization of RF power amplifiers," *IEEE Microw. Wireless Technol. Lett.*, vol. 33, no. 9, pp. 1357–1360, Sep. 2023.

[15] X. Hu et al., "Convolutional neural network for behavioral modeling and predistortion of wideband power amplifiers," *IEEE Trans. Neural Netw. Learn. Syst.*, vol. 33, no. 8, pp. 3923–3937, Aug. 2022.

[16] T. Kobal, Y. Li, X. Wang, and A. Zhu, "Digital predistortion of RF power amplifiers with phase-gated recurrent neural networks," *IEEE Trans. Microw. Theory Techn.*, vol. 70, no. 6, pp. 3291–3299, Jun. 2022.

[17] D. Wang, M. Aziz, M. Helaoui, and F. M. Ghannouchi, "Augmented real-valued time-delay neural network for compensation of distortions and impairments in wireless transmitters," *IEEE Trans. Neural Netw. Learn. Syst.*, vol. 30, no. 1, pp. 242–254, Jan. 2019.

[18] G. Mouginot, R. Sommet, R. Quéré, Z. Ouarch, S. Heckmann, and M. Camiade, "Thermal and trapping phenomena assessment on AlGaN/GaN microwave power transistor," in *Proc. 5th Eur. Microw. Integr. Circuits Conf.*, Sep. 2010, pp. 110–113. [Online]. Available: https://ieeexplore.ieee.org/document/5613754

[19] J. C. Pedro, P. M. Cabral, T. R. Cunha, and P. M. Lavrador, "A multiple time-scale power amplifier behavioral model for linearity and efficiency calculations," *IEEE Trans. Microw. Theory Techn.*, vol. 61, no. 1, pp. 606–615, Jan. 2013.

[20] A. S. Tehrani, T. Eriksson, and C. Fager, "Modeling of long term memory effects in RF power amplifiers with dynamic parameters," in *IEEE MTT-S Int. Microw. Symp. Dig.*, Jun. 2012, pp. 1–3.

[21] F. M. Barradas, L. C. Nunes, T. R. Cunha, P. M. Lavrador, P. M. Cabral, and J. C. Pedro, "Compensation of long-term memory effects on GaN HEMT-based power amplifiers," *IEEE Trans. Microw. Theory Techn.*, vol. 65, no. 9, pp. 3379–3388, Sep. 2017.

[22] P. M. Tomé, F. M. Barradas, T. R. Cunha, and J. C. Pedro, "Hybrid analog/digital linearization of GaN HEMT-based power amplifiers," *IEEE Trans. Microw. Theory Techn.*, vol. 67, no. 1, pp. 288–294, Jan. 2019.

[23] L. Chen, W. Chen, Y. Wang, and Z. Feng, "Linearization of GaN HEMT-based power amplifiers using a bias tracking digital predistortion," in *IEEE MTT-S Int. Microw. Symp. Dig.*, May 2021, pp. 1–3.

[24] F. M. Barradas, P. M. Tomé, T. R. Cunha, and J. C. Pedro, "Compensation of power amplifier long-term memory behavior for pulsed radar applications," *IEEE Trans. Microw. Theory Techn.*, vol. 67, no. 12, pp. 5249–5256, Dec. 2019.

[25] Y. Yu, L. Yu, P. Chen, and C. Yu, "Behavioral modeling of millimeter wave GaN power amplifiers for 6G integrated sensing and communications application," in *IEEE MTT-S Int. Microw. Symp. Dig.*, Jun. 2024, pp. 653–656.

[26] Q. Zhang, C. Jiang, G. Yang, R. Han, and F. Liu, "Multi-output recurrent neural network behavioral model for digital predistortion of RF power amplifiers," *IEEE Microw. Wireless Technol. Lett.*, vol. 33, no. 7, pp. 1067–1070, Jul. 2023.

[27] Q. Zhang, C. Jiang, G. Yang, R. Han, and F. Liu, "Block-oriented recurrent neural network for digital predistortion of RF power amplifiers," *IEEE Trans. Microw. Theory Techn.*, vol. 72, no. 7, pp. 3875–3885, Jul. 2024.

[28] S. Fakhfakh, A. Martin, M. Campovecchio, G. Neveux, and D. Barataud, "On-wafer time-domain and low-frequency measurements of GaN HEMTs for accurate trap modeling and its impact on pulse-to-pulse stability," in *Proc. Int. Workshop Integr. Nonlinear Microw. Millimetre-Wave Circuits (INMMIC)*, Jul. 2018, pp. 1–3.

[29] P. M. McCormick, C. Sahin, S. D. Blunt, and J. G. Metcalf, "FMCW implementation of phase-attached radar-communications (PARC)," in *Proc. IEEE Radar Conf.*, Apr. 2019, pp. 1–6.

[30] J. Chani-Cahuana, P. N. Landin, C. Fager, and T. Eriksson, "Iterative learning control for RF power amplifier linearization," *IEEE Trans. Microw. Theory Techn.*, vol. 64, no. 9, pp. 2778–2789, Sep. 2016.

[31] Y. Yu, P. Chen, X.-W. Zhu, J. Zhai, and C. Yu, "Continual learning digital predistortion of RF power amplifier for 6G AI-empowered wireless communication," *IEEE Trans. Microw. Theory Techn.*, vol. 70, no. 11, pp. 4916–4927, Nov. 2022.

[32] R.-J. Liu et al., "A 24–28-GHz GaN MMIC synchronous Doherty power amplifier with enhanced load modulation for 5G mm-wave applications," *IEEE Trans. Microw. Theory Techn.*, vol. 70, no. 8, pp. 3910–3922, Aug. 2022.

[33] A. S. Tehrani, H. Cao, S. Afsardoost, T. Eriksson, M. Isaksson, and C. Fager, "A comparative analysis of the complexity/accuracy tradeoff in power amplifier behavioral models," *IEEE Trans. Microw. Theory Techn.*, vol. 58, no. 6, pp. 1510–1520, Jun. 2010.


**Yucheng Yu** (Graduate Student Member, IEEE) received the B.E. degree in information science and engineering from Southeast University, Nanjing, China, in 2020, where he is currently pursuing the Ph.D. degree at the State Key Laboratory of Millimeter Waves.

His current research interests include nonlinear behavioral modeling and digital predistortion for RF power amplifiers and millimeter-wave beamforming transmitters.

**Luqi Yu** (Graduate Student Member, IEEE) was born in Zibo, Shandong, China, in 1999. He received the B.E. degree in electronic communication engineering from Nanjing University of Science and Technology, Nanjing, China, in 2021. He is currently pursuing the Ph.D. degree at the State Key Laboratory of Millimeter Waves, Southeast University, Nanjing.

His current research interests include broadband high-efficiency gallium nitride (GaN) power amplifier (PA) design and GaN monolithic microwave integrated circuit (MMIC) PA design for RF/microwave and millimeter-wave applications.

**Ruijia Liu** (Member, IEEE) received the B.E. degree in electronic information science and technology from Southwest Jiaotong University (SWJTU), Chengdu, China, in 2017, and the Ph.D. degree in electromagnetic field and microwave technology from Southeast University (SEU), Nanjing, China, in 2022.

From October 2022 to August 2024, he was a Post-Doctoral Research Fellow at the RF and Microwave Research Group, University College Dublin (UCD), Dublin, Ireland. He is currently an Assistant Professor with the School of Electrical and Electronic Engineering, UCD. His research interests include broadband high-efficiency gallium nitride (GaN) power amplifier (PA) design and GaN monolithic microwave integrated circuit PA design for RF/microwave and millimeter-wave applications.

**Xiao-Wei Zhu** (Member, IEEE) received the M.E. and Ph.D. degrees in electronic and information engineering from Southeast University, Nanjing, China, in 1996 and 2000, respectively.

Since 1984, he has been with Southeast University, where he is currently a Professor with the School of Information Science and Engineering. He has authored or co-authored more than 100 technical publications. He holds more than 25 patents. His current research interests include radio frequency and antenna technologies for wireless communications, microwave and millimeter-wave theory and technology, and also power amplifier (PA) nonlinear characteristics and its linearization research with a particular emphasis on wideband and high-efficiency gallium nitride (GaN) PAs.

Dr. Zhu was a recipient of IEEE Microwave Theory and Techniques Society 2021 Microwave Prize and the 2003 Second-Class Science and Technology Progress Prize of Jiangsu Province, China.

**Peng Chen** (Member, IEEE) received the B.E. degree in communication engineering and the M.E. degree in electronic engineering from Harbin Institute of Technology, Harbin, China, in 2010 and 2012, respectively, and the Ph.D. degree in electronic engineering from University College Dublin, Dublin, Ireland, in 2016.

From 2017 to 2020, he was a Research Associate with the Centre for High Frequency Engineering, Cardiff University, Cardiff, U.K. Since October 2020, he has been with the School of Information Science and Engineering, Southeast University, Nanjing, China, where he is currently a Lecturer. His current research interests include nonlinear device modeling and optimization of hybrid and integrated power amplifiers.

**Chao Yu** (Senior Member, IEEE) received the B.E. degree in information engineering and the M.E. degree in electromagnetic fields and microwave technology from Southeast University (SEU), Nanjing, China, in 2007 and 2010, respectively, and the Ph.D. degree in electronic engineering from University College Dublin (UCD), Dublin, Ireland, in 2014.

He is currently a Professor with the State Key Laboratory of Millimeter Waves, School of Information Science and Engineering, SEU, and Purple Mountain Laboratories, Nanjing. His current research interests include microwave and millimeter-wave power amplifier modeling and linearization, and 5G massive multiple-input–multiple-output (MIMO) radio frequency (RF) system design.